Received: 24 May 2024 | Revised: 20 September 2024 | Accepted: 28 October 2024 | Published online: 11 November 2024

RESEARCH ARTICLE

Archives of Advanced Engineering Science
2024, Vol. 00(00) 1–9
DOI: 10.47852/bonviewAAES42023485

BON VIEW PUBLISHING

Influence of Airfoil Geometry on VTOL UAV Aerodynamics at Low Reynolds Numbers

Timothy A. Adeyi[1], Oluwaseyi O. Alabi[1,*] and Olumide A. Towoju[1]

[1]*Department of Mechanical Engineering, Lead City University, Nigeria*

Abstract: This study examines the impact of airfoil geometry on the aerodynamic properties of a low Reynolds number flying wing unmanned aerial vehicle (UAV). The investigation was conducted at three Reynolds numbers (1×10^6, 2×10^6, and 5×10^6), all under a constant Mach number of 0.3 during subsonic flight. Four distinct airfoils from the NACA and Selig series were analyzed using XFLR5 v6.61, with the angle of attack varying from −5° to 15°. Among the airfoils, NACA 6409 consistently demonstrated superior aerodynamic performance across all Reynolds numbers. Notably, at a Reynolds number of 1×10^6, NACA 6409 achieved a peak lift coefficient (Cl) of 1.584 at an angle of attack of 11.1°, indicating high efficiency. Additionally, the study explored the angles of attack where the drag coefficient (Cd) increased sharply, as well as the lift-to-drag ratios (Cl/Cd), providing a comprehensive understanding of stalling behavior and the balance between lift and drag. These findings offer valuable insights into the aerodynamic efficiency of airfoils in the context of vertical takeoff and landing (VTOL) UAV design, underscoring the importance of further research to optimize airfoil designs for enhanced VTOL UAV performance.

Keywords: angle of attack, NACA series, Selig airfoils, XFLR5 simulation, lift-to-drag ratio

1. Introduction

Vertical takeoff and landing (VTOL) unmanned aerial vehicles (UAVs) are transforming aviation by fusing versatility and operational efficiency. Owing to their unique ability to ascend and descend vertically, these airborne platforms function without using conventional runways. Simply put, VTOL UAVs extend the boundaries of aerial mobility and offer unparalleled versatility for a variety of applications [1]. Because of their versatility, VTOL UAVs can be employed for a variety of missions, such as logistics, reconnaissance, and surveillance. They are vital tools in both the military and civilian sectors due to their adaptability to a wide range of operating environments. VTOL UAVs exhibit an astounding range of uses that surpass the capabilities of conventional aircraft, whether they are utilized for maneuvering through intricate urban environments or for reaching distant and difficult terrains [2, 3]. The variety of VTOL UAVs, from quadcopters to tilt rotors, each designed to fulfill a particular mission need, further emphasizes this diversity [4, 5]. VTOL capabilities are becoming increasingly popular due to their inherent advantages, which include faster deployment times, less infrastructure needed, and improved agility in tight locations. VTOL UAVs are therefore distinct from traditional fixed-wing or rotorcraft, which makes them vital in situations where accessibility and agility are critical.

The effectiveness of VTOL UAVs is dependent on several factors, one of which is airfoil geometry—the shape and arrangement of an airfoil. The aerodynamic performance of these aircraft is largely determined by the shape and configuration of the airfoil, especially at low Reynolds (Re) numbers. Re numbers are a dimensionless quantity used to predict the nature of fluid flow, whether it is laminar or turbulent. This study specifically aims to investigate the flow around various asymmetric airfoils from two airfoil families—NACA and Selig—to determine the aerodynamic differences, similarities, and the effect of shape on aerodynamic parameters.

Four airfoils—NACA 6409, NACA 65410, NACA 4412, and Selig 1091—that were chosen for VTOL UAV applications are thoroughly examined in this study. The study examines the aerodynamic properties of these airfoils at low Re numbers using computational fluid dynamics (CFD) simulations, emphasizing lift, drag, and moment coefficients at different angles of attack (AOA). This study does not take turbulent effects into account to simplify the analysis. The results are verified by comparing them with existing literature, offering fresh insight into the aerodynamic performance of these airfoils and guiding optimization tactics for VTOL UAV design.

Scholars have explored the complex relationship between aerodynamic performance and airfoil design, notably [6], whose work highlights the impact of various airfoil geometries on VTOL UAV aerodynamics [4, 7–9]. However, despite the extensive research on airfoil aerodynamic performance, a direct comparison of the aerodynamic characteristics of NACA 6409, NACA 65410, NACA 4412, and Selig 1091 airfoils has not been conducted [10]. This study addresses this gap by providing a comparative analysis of these airfoils, thereby contributing to the ongoing development of UAV technology.

*Corresponding author: Oluwaseyi O. Alabi, Department of Mechanical Engineering, Lead City University, Nigeria. Email: alabi.oluwaseyi@lcu.edu.ng

Concurrently, the evolution of VTOL UAVs over time demonstrates advancements in aerospace technology. Early initiatives laid the foundation for modern platforms [4, 5, 11–13]. Significant progress was made in the 20th century with the advent of tiltrotor aircraft like the V-22 Osprey, which marked a pivotal point in the history of VTOL [14]. UAV platforms were revolutionized by the addition of VTOL capabilities, providing strategic advantages, particularly in military reconnaissance [15–17]. As VTOL UAVs continue to evolve, optimizing airfoil geometries for efficient performance becomes increasingly important, underscoring the need for this comprehensive comparison of aerodynamic characteristics presented in this study.

A detailed summary of the various airfoil properties for the chosen geometries—NACA 6409, NACA 65410, NACA 4412, and Selig 1091—is provided in Table 1. Analysis of the thickness percentages reveals differences between 5.06% and 12.00%, each precisely correlated with specific maximum thickness points along the chord, ranging from 13.42% to 40.04%. This variation in thickness distribution influences the distinct aerodynamic properties of each airfoil geometry.

The interaction between historical evolution, technological advancements, and the subtleties of airfoil design provides a holistic depiction of the complex terrain surrounding VTOL UAVs [18, 19]. This journey reflects the ongoing pursuit of efficiency, adaptability, and performance in unmanned aerial systems, from the early efforts that laid the groundwork to the revolutionary incorporation of VTOL capabilities in modern platforms. By addressing a significant research gap, this study contributes valuable insights into VTOL UAV technology, enhancing our understanding of airfoil geometries and their impact on aerodynamic performance.

The aerodynamic performance of VTOL UAVs at low Re numbers is highly dependent on the geometry of the airfoil used. However, the current understanding of this relationship is limited, which hinders the development of more efficient VTOL UAV designs. This study not only provides valuable insights into the relationship between airfoil geometry and aerodynamic performance but also paves the way for future research to explore additional factors, such as wing shape and orientation, on aerodynamic performance at low Re numbers.

2. Methodology

The selection of airfoils for simulation analysis—NACA 6409, NACA 65410, NACA 4412, and Selig 1091—was driven by their established high lift and low drag characteristics, specifically chosen for their suitability in VTOL UAVs. This consideration prioritized low Re numbers and the low flight speed range typical of subsonic aircraft design [20]. Re numbers of 1×10^6, 2×10^6, and 5×10^6 were used for the simulation parameters, as they lie within the recognized range for legitimate aerodynamic models [21]. To represent actual operating conditions, the anticipated Mach number was kept at 0.3 [22]. Type 1 analysis using structured meshing produced by the "SAGE" algorithm and XFLR5 v 6.61 software, a tool that uses the XFoil program to compute the aerodynamic properties of airfoils, were both used in the analysis. This approach was selected because it may be used to examine aerodynamic characteristics at low speeds [23, 24].

The numerical simulations performed using the open-source software XFLR5 v6.61 were based on the Cebeci-Smith turbulence model. The software uses a finite volume approach to solve the governing equations for incompressible flow, and applies a second-order upwind scheme to discretize the convective terms. The solution algorithm is based on the SIMPLEC (Semi-Implicit Method for Pressure Linked Equations Consistent) method, and the turbulence model was validated by comparing the predictions with experimental data from the literature. The simulations were carried out with a total of 27114 panels, with 125 bound vortex X-axis direction and 106 Y-axis direction at wing. This process was used to analyze the aerodynamic forces, including lift coefficient (Cl), drag coefficient (Cd), and efficiency (Cl/Cd).

During the simulation, the main metrics that were investigated were Cls, Cds, AOA, and lift-to-drag ratio. When taken as a whole, these parameters offered a thorough insight of the airfoil performance. The range of AOA covered by the simulation was −5° to 15° in order to capture a wide variety of aerodynamic behavior. This range included both positive and negative AOA, providing important information about the performance of the airfoils. Moreover, it matched the typical AOA values found in subsonic flight, which increased the findings' applicability to practical situations.

In order to guarantee a reliable analysis, the airfoils and simulation parameters that were used were carefully chosen, taking into account the unique aerodynamic conditions connected to low Re numbers and low-speed flying, as well as their suitability for VTOL UAVs. By using this method, the simulation results become more reliable and practically relevant, and they offer insightful information that may be used to optimize airfoil designs for VTOL UAVs. The selection of airfoils for simulation analysis—NACA 6409, NACA 65410, NACA 4412, and Selig 1091—was driven by their established high lift and low drag characteristics, specifically chosen for their suitability in VTOL UAVs. This consideration prioritized low Re numbers and the low flight speed range typical of subsonic aircraft design [20].

A Re number of 1×10^6, 2×10^6, and 5×10^6 were used for the simulation parameters, as they lie within the recognized range for legitimate aerodynamic models. To represent actual operating conditions, the anticipated Mach number was kept at 0.3 [22]. Type 1 analysis using structured meshing produced by the "SAGE" algorithm and XFLR5 v 6.61 software, a tool that uses the XFoil program to compute the aerodynamic properties of airfoils, were both used in the analysis. This approach was selected because it may be used to examine aerodynamic characteristics at low speeds [23, 24].

The numerical simulations performed using the open-source software XFLR5 v 6.61 were based on the Cebeci-Smith turbulence model. The software uses a finite volume approach to solve the governing equations for incompressible flow and applies a second-order upwind scheme to discretize the convective terms. The solution algorithm is based on the SIMPLEC method, and the turbulence model was validated by comparing the predictions with experimental data from the literature. The simulations were carried out with a total of 27114 panels, with 125 bound vortex X-axis direction and 106 Y-axis direction at wing. This process was used to analyze the aerodynamic forces, including Cl, Cd, and efficiency (Cl/Cd).

During the simulation, the main metrics that were investigated were Cls, Cds, AOA, and lift-to-drag ratio. When taken as a whole, these parameters offered a thorough insight of the airfoil performance. The range of AOA covered by the simulation was −5° to 15° in order to capture a wide variety of aerodynamic behavior. This range included both positive and negative AOA, providing important information about the performance of the airfoils. Moreover, it matched the typical AOA values found in subsonic flight, which increased the findings' applicability to practical situations.

Table 1
Airfoil parameters of the chosen geometries

Airfoil parameters	NACA 6409	NACA 65410	NACA 4412	Selig 1091
Thickness (%)	9.00	9.99	12.00	5.06
Max. Thickness Position (%)	29.03	40.04	29.03	13.42
Max. Camber (%)	6.00	2.21	4.00	6.06
Max. Camber Position (%)	39.54	50.05	39.54	45.15
Number of Panels	99	51	99	81

In order to guarantee a reliable analysis, the airfoils and simulation parameters that were used were carefully chosen, taking into account the unique aerodynamic conditions connected to low Re numbers and low-speed flying, as well as their suitability for VTOL UAVs. By using this method, the simulation results become more reliable and practically relevant, and they offer insightful information that may be used to optimize airfoil designs for VTOL UAVs. The purpose of this simulation analysis is to investigate the aerodynamic performance of four airfoils (NACA 6409, NACA 65410, NACA 4412, and Selig 1091) for VTOL UAVs, to identify the optimal airfoil design for efficient lift and drag characteristics. By conducting this analysis, we aim to contribute to the development of more efficient and effective VTOL UAVs, which have the potential to revolutionize various fields such as aerial reconnaissance, search and rescue, and cargo transport.

In addition to geometric factors, the range of panel counts (from 51 to 99) highlights the structural details that are critical to the aerodynamic evaluations carried out in this study. The need for a fine-grained structural representation to effectively depict the subtleties of aerodynamic performance is reflected in the variance in panel counts among the various airfoils. This thorough analysis of the airfoil properties in Table 1 helps to a sophisticated understanding of the unique qualities displayed by each airfoil geometry and establishes a strong basis for the ensuing aerodynamic analyses. The configurations of the four airfoils and the airfoil geometries for the chosen candidates are depicted in Figures 1 and 2, respectively. When we explore the maximum camber range, we find values from 2.21% to 6.06%. The chord's maximum camber locations vary between 39.54% and 50.05%. With its smaller thickness and distinctive camber characteristics-registering at 5.06% and 6.06%, respectively, the Selig 1091 airfoil stands out. Each airfoil shape has unique camber and thickness profiles, which highlights the intricate design considerations that go into each one.

2.1. Governing equations

The incompressible Navier-Stokes equation is used in a time-dependent, conservative version by the solver, which is criticized using a finite volume method. The incompressible Navier-Stokes equations in tensor form are as follows:

$$\frac{\partial U_i}{\partial x_i} = 0 \tag{1}$$

$$\frac{\partial U_i}{\partial t} + \frac{\partial (U_i U_j)}{\partial x_j} = -\frac{1}{\rho}\frac{\partial P}{\partial x_i} + \nu \frac{\partial}{\partial x_j}\left(\frac{\partial U_i}{\partial x_j}\right) \tag{2}$$

The x, y, and z directions are represented by the indices $i = 1, 2$, and 3, respectively, while the U_1, U_2, and U_3 designate the velocity components, which correspond to U, V, and W, respectively. With the proper length and velocity scale, the equations are non-dimensionalized. Cell-centered, non-staggered arrangement is used to discretize the Navier-Stokes equations. The face-center velocities are computed and used to determine the volume flux of each cell, in addition to the cell-center velocities. The equation of tensor in Equation (2) is written as:

$$\frac{\partial U_i}{\partial t} + \frac{\partial (U_i U_j)}{\partial x_j} = -\frac{\partial P}{\partial x_i} + \frac{1}{Re}\frac{\partial^2 U_i}{\partial x_j\, x_j} \tag{3}$$

$$\frac{\partial U_i}{\partial x_j} = 0 \tag{4}$$

where Re is the Reynolds number and it is expressed as:

$$R_e = \frac{\rho U_o D}{\mu} \tag{5}$$

where ρ, U_o, μ and D are the density, velocity of the fluid, dynamic viscosity of the fluid, and the characteristic length of the airfoil, respectively.

3. Results

Table 2 provides a comprehensive summary of the airfoil geometries and their respective stall angles, whereas Table 1 displays the geometrical parameters of the four chosen airfoils. This data is helpful in assessing the airfoils' aerodynamic performance. A closer look at maximum Cls reveals unique properties for every airfoil. Specifically, at an AOA of 11.1°, NACA 6409 reaches a maximum Cl of 1.584181, whereas, at 9.3°, NACA 65410 shows a maximum Cl of 1.084181. Comparably, Selig 1091 displays a maximum Cl of 1.678985 at 10.9°, and NACA 4412 shows a peak Cl of 1.547063 at 13.5°. These results provide important new information about the relative aerodynamic performance of the chosen airfoil geometries.

By showing the distribution of lift and Cds with respect to the AOAs, Figure 3 improves our understanding. Certain values are found for each airfoil when the AOA at which the Cd increases quickly is analyzed. This event is seen at 1.40° in NACA 6409, −0.3° in NACA 65410, 1.3° in NACA 4412, and 1.9° in Selig 1091. These data are essential for understanding the stalling behavior that each airfoil geometry under investigation exhibits. Using a comprehensive method to assess overall aerodynamic performance at these specific Re numbers, Figure 4 shows the analysis of the lift-to-drag ratio (Cl/Cd). The graph portrays the distribution of the lift-to-drag ratio with respect to the AOA. Noteworthy findings include NACA 6409 achieving a maximum Cl/Cd of 152.6566 at an AOA of 5.2°, NACA 65410 exhibiting a peak value of 101.528 at 1.8°, NACA 4412 demonstrating a

Figure 1
Airfoil geometries for the selected candidates

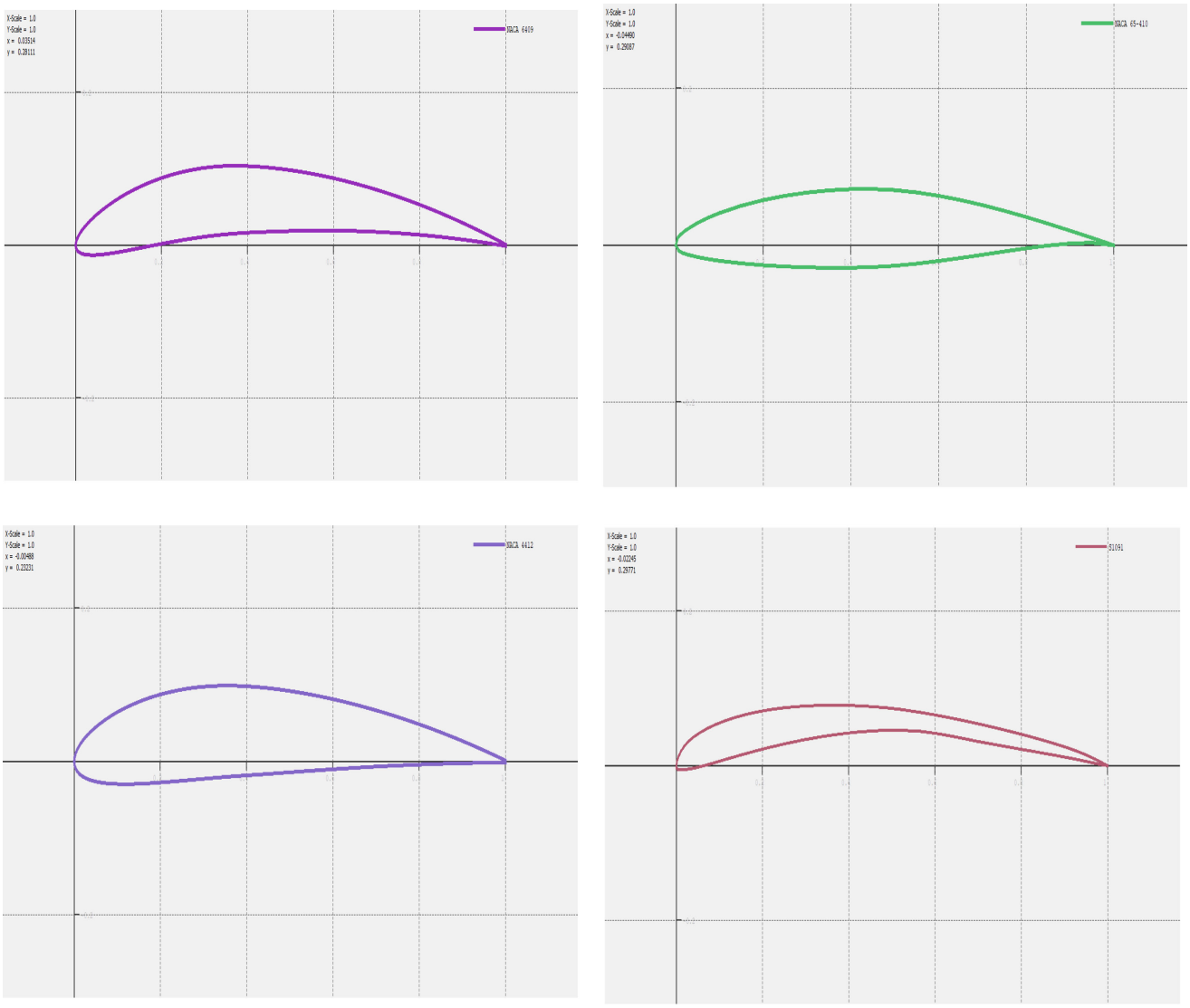

Figure 2
Configurations of the four airfoils

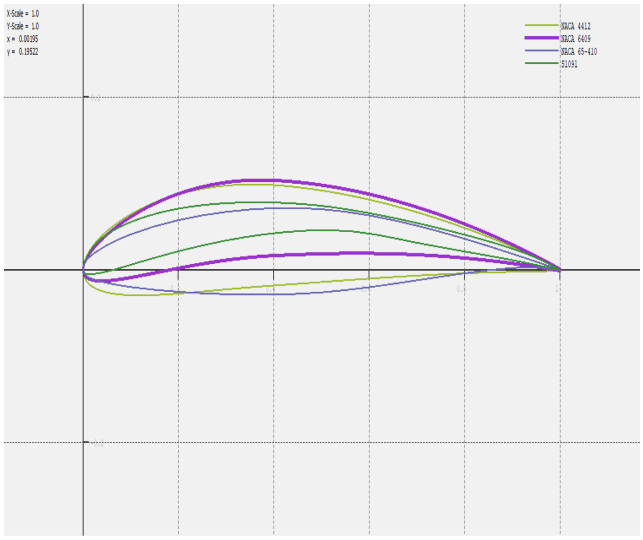

maximum Cl/Cd of 133.1235 at 5.5º, and Selig 1091 showcasing a value of 138.8621 at 3.1º.

Figure 5 shows the variations of lift and Cds with the corresponding AOAs for the four distinct airfoil geometries at a Re number of 2×10^6 and a Mach number of 0.3, the critical parameters of interest which are the AOA at drag divergence, maximum coefficient of lift (Cl), and lift-to-drag ratio (Cl/Cd) are quite obvious. Examining the results in Table 3 which is the Xfoil

Table 2
Xfoil results at Re = 1×10^6

Airfoil	Re = 1×10^6	
	α_{stall}	$c_{l\ max}$
NACA **6409**	11.1º	1.584181
NACA **65410**	9.3º	1.084181
NACA **4412**	13.5º	1.547063
Selig 1091	10.9º	1.678985

Figure 3
Lift and drag coefficient distribution with the angle of attack at Re = 1 × 10⁶. (a) Coefficient of Lift vs AOA for Re = 1E6. (b) Coefficient of Drag vs AOA for Re = 1E6

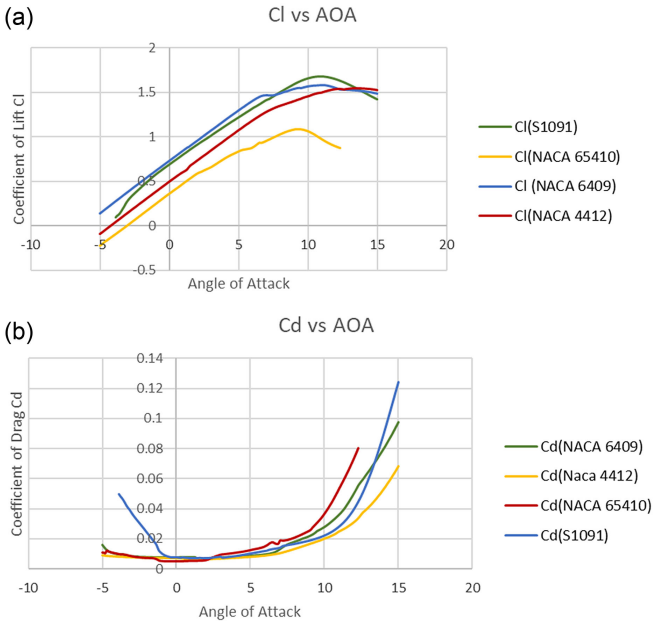

Figure 4
Lift-to-drag coefficient distribution with the angle of attack at Re = 1 × 10⁶

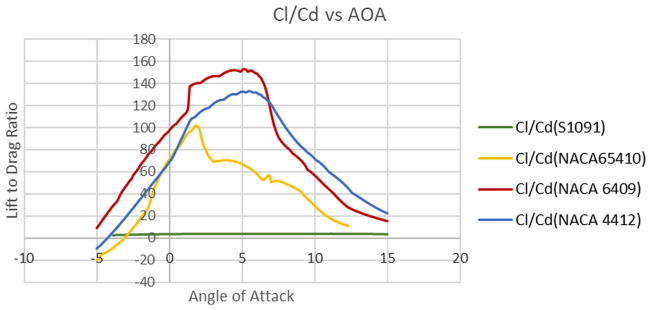

result at Re numbers 2×10^6, the stall AOA (α_{stall}), and maximum lift coefficient (Cl_{max}) for each airfoil geometry are noteworthy. NACA 4412 demonstrates the highest stall angle at 14.4°, while NACA 65410 exhibits the lowest at 9.2°. Regarding Cl_{max}, NACA 6409 achieves the highest value at 1.684176.

Furthermore, the critical transition in drag characteristics, as observed in Cd vs AOA, is elucidated. At a Re number of 2×10^6, NACA 6409 experiences a drastic increase in drag (Cd = 0.005773) at 2.1°, while NACA 65410, NACA 4412, and Selig 1091 encounter similar transitions at 0.2°, 2.2°, and –0.3°, respectively. The assessment of aerodynamic efficiency, expressed as Cl/Cd, shown in Figure 6 offers valuable insights. NACA 6409 exhibits the highest efficiency at 184.8392, occurring at 4.8°,

Figure 5
Lift and drag coefficient distribution with the angle of attack at Re = 2 × 10⁶. (a) Coefficient of lift vs AOA for Re = 2E6. (b) Coefficient of drag vs AOA for Re = 2E6

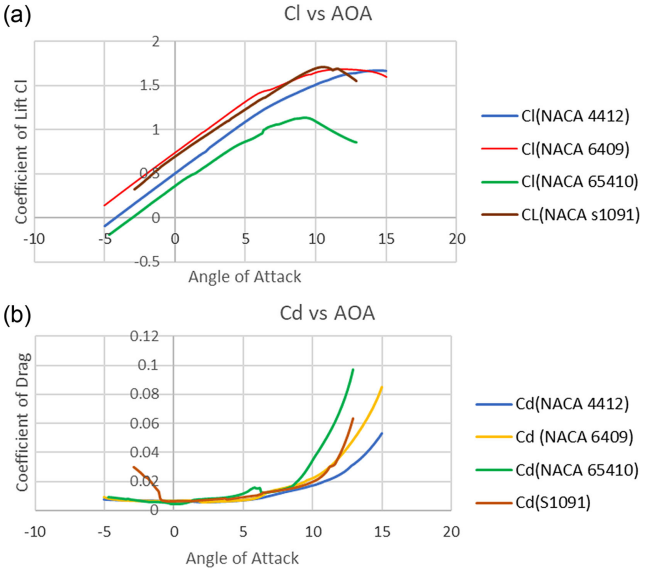

Table 3
Xfoil results at Re = 2 × 10⁶

Airfoil	Re = 2 × 10 ⁶	
	α_{stall}	Cl_{max}
NACA **6409**	11.9°	1.684176
NACA **65410**	9.2°	1.135134
NACA **4412**	14.4°	1.66922
Selig 1091	10.5°	1.711012

Figure 6
Lift-to-drag coefficient distribution with the angle of attack at Re = 2 × 10⁶

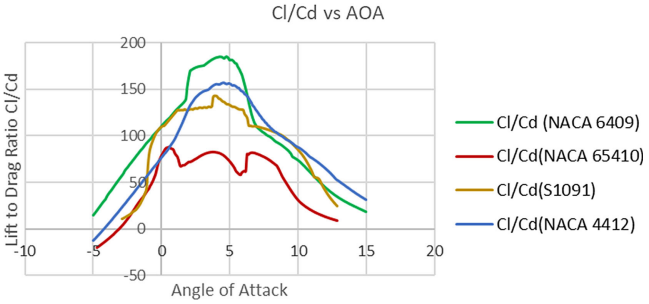

Figure 7
Lift and drag coefficient distribution with the angle of attack at Re = 5 × 10⁶. (a) Coefficient of lift vs AOA for Re = 5E6. (b) Coefficient of drag vs AOA for Re = 5E6

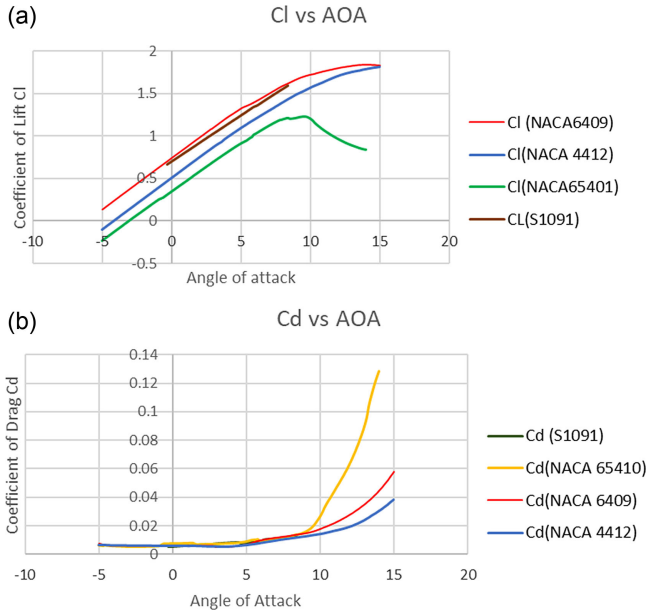

emphasizing its favorable balance between lift and drag. Meanwhile, NACA 65410, NACA 4412, and Selig 1091 showcase their optimum efficiencies at 0.6°, 4.5°, and −4.0°, respectively. The aerodynamic performance of the airfoils undergoes significant changes at a Re number of 5 × 10⁶, as illustrated in Figure 7. NACA 4412 has the highest stall AOA at 15°, while NACA 65410 has the lowest at 9.6°. NACA 6409 achieves the highest Cl_{max}, while the other airfoils exhibit lower Cl_{max}. The Cd increases sharply for each airfoil at a specific AOA, with NACA 6409 reaching the highest value at 2.9°.

At a Re number of 5 × 10⁶, the aerodynamic performance of the airfoil geometries undergoes notable changes. Examining Table 4, the stall AOA (α_{stall}) and Cl_{max} reveals compelling insights. NACA 4412 exhibits the highest stall angle at 15°, while NACA 65410 has the lowest at 9.6°. NACA 6409 achieves the highest Cl_{max} at 1.838532.

Table 4
Xfoil results at Re = 5 × 10⁶

	Re = 5 × 10⁶	
Airfoil	α_{stall}	C_{lmax}
NACA 6409	13.9°	1.838532
NACA 65410	9.6°	1.226276
NACA 4412	15°	1.817686
Selig 1091	8.4°	1.594155

Analyzing Cd vs AOA, significant increases in drag become evident at specific angles for each airfoil geometry. Notably, NACA 6409 experiences a drastic rise in drag (Cd = 0.005023) at 2.9°, while NACA 65410, NACA 4412, and Selig 1091 encounter similar transitions at −0.2°, 3.6°, and −0.2° respectively.

Figure 8
Lift-to-drag coefficient distribution with the angle of attack at Re = 5 × 10⁶

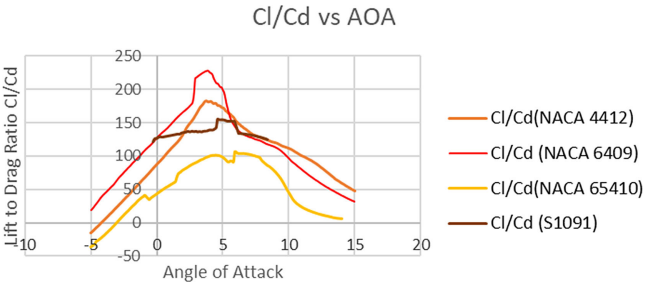

The evaluation of aerodynamic efficiency, expressed as Cl/Cd, Figure 8 provides further insights to the performance of the geometries. NACA 6409 exhibits the highest efficiency at 228.0396, occurring at 3.8°, emphasizing its superior balance between lift and drag. NACA 4412, NACA 65410, and Selig 1091 showcase their optimum efficiencies at 3.7°, 5.9°, and 4.6° respectively.

The comparative analysis of the results of simulation from each Re number (1 × 10⁶, 2 × 10⁶, and 5 × 10⁶) provides a comprehensive understanding of how airfoil geometries perform under varying aerodynamic conditions for subsonic flight in VTOL UAV design.

Figure 9 depicts the Cl and lift-to-drag ratio (Cl/Cd) of each airfoil at different AOA, for various Re numbers. The Cl increases with increasing AOA for all airfoils, with the exception of NACA 6409. The reason for this deviation from the general trend is not clear. It is also observed that the Cl/Cd ratio increases with increasing Re number, for all airfoils and AOAs. At high Re numbers, however, the Cl/Cd ratio drops with increasing AOA, suggesting a decline in aerodynamic efficiency. These patterns align with other academics' findings.

The results for Cl_{max} and stall angles at a Re number of 1 × 10⁶ reveal unique characteristics for every airfoil geometry. NACA 6409 exhibits superior efficiency throughout a range of Re numbers, as evidenced by its consistent achievement of higher Cl_{max} than the other airfoils. Figure 3's examination of drag divergence provides information about the critical angles of attack at which each airfoil experiences a sudden rise in drag, providing insight into the stalling behavior of the individual airfoils. Understanding this data is crucial for comprehending the airfoils' aerodynamic performance.

The impact of the Re number of 2 × 10⁶ on airfoil performance is demonstrated in the second set of findings. Notably, NACA 6409 attains the highest Cl_{max} while NACA 4412 displays the largest stall angle. The crucial transitions in drag for each airfoil are highlighted by the drag against AOA (Cd vs AOA) analysis, which provides important insights into the aerodynamic behavior of the airfoils. The analysis of aerodynamic efficiency (Cl/Cd) emphasizes the significance of maintaining a balance between lift and drag, with NACA 6409 showing the highest efficiency.

The findings show that an airfoil's performance significantly changes at a Re number of 5 × 10⁶. NACA 4412 still has the highest stall angle, but NACA 6409 is still the airfoil with the highest Cl_{max}. The measurement of Cd versus AOA reveals notable increases in drag for every airfoil at particular angles. These findings highlight NACA 6409's improved aerodynamic efficiency even at higher Re numbers.

Significant insights into the aerodynamic properties of various airfoil shapes, such as NACA 6409, NACA 65410, NACA 4412, and Selig 1091, have been obtained by the analysis of a variety of low Re

Figure 9
Lift coefficients and Cl/Cd of the airfoil geometries. (a) Cl vs AOA for NACA 4412. (b) Cl/Cd vs AOA for NACA 4412. (c) Cl vs AOA for NACA 6409. (d) Cl/Cd vs AOA for NACA 6409. (e) Cl vs AOA for NACA 65410. (f) Cl/Cd vs AOA for NACA 65410. (g) Cl vs AOA for S 1019. (h) Cl/Cd vs AOA for the S 1019

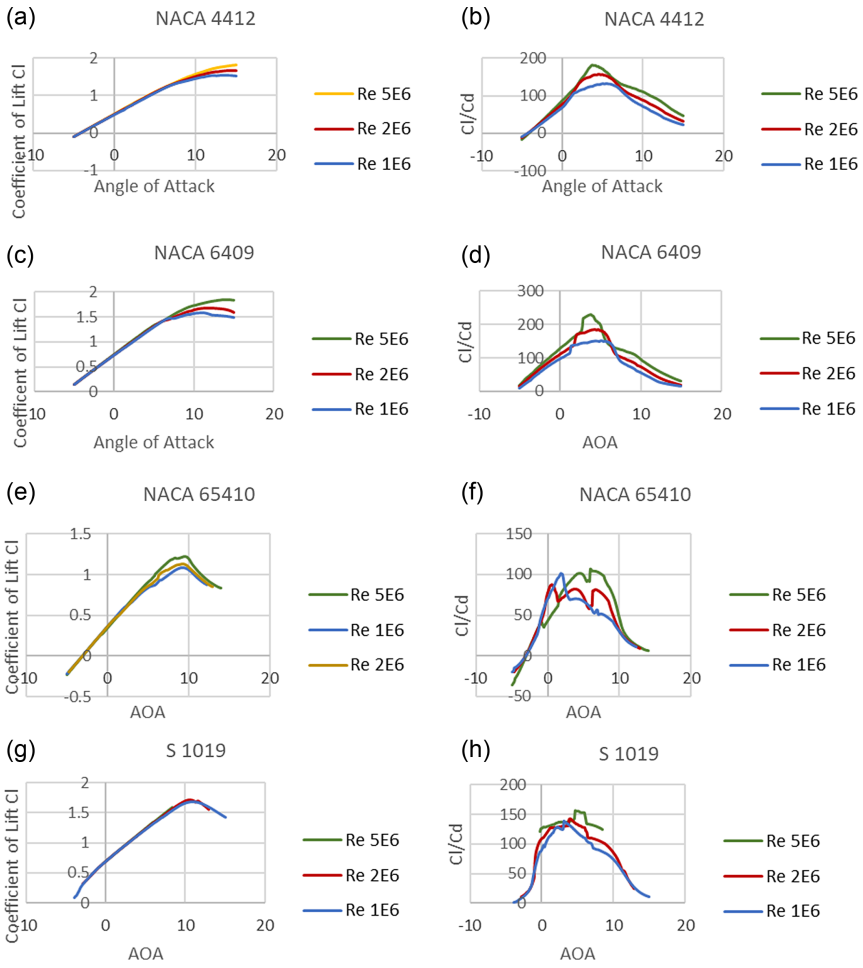

numbers (1×10^6, 2×10^6, and 5×10^6) at these airfoil geometries. In particular, the results for NACA 6409 at Re numbers 1×10^6 and 2×10^6 exhibit a stable trend that is in line with the information released by Jones et al. [11]. The results of the study are largely consistent with those reported by Maji et al. [21], with one notable difference being the lower lift-to-drag ratio for NACA 4412, which is different from the higher lift-to-drag ratio reported by Jones et al. [11] for the same airfoil.

Beyond these differences, a recurring pattern up until it reaches particular values that are particular to each geometry, the Cl rises steadily before declining. This observed result highlights the complex link between airfoil geometry and aerodynamic performance and is consistent with published findings in the literature [11]. Significantly, this behavior emphasizes how important AOA is in determining Cls, illustrating the intricate relationship between design features and aerodynamic results. The different lift-to-drag ratios of NACA 4412 and 6409 highlight how aerodynamic performance is sensitive to even small changes in airfoil design. NACA 4412 deviates from this trend, but NACA 6409 shows a steady pattern in the lift-to-drag ratio at various Re numbers. Maji et al. [21] emphasized that this disparity highlights the necessity for a comprehensive understanding of the effect of particular design variants on the overall aerodynamic efficiency of airfoils.

The results of the XFLR5 v 6.61 simulations for the NACA 4412 airfoil were validated by comparing them to two experimental studies: Haque et al. [25] and Mehdi et al. [26]. The results for the NACA 6409 airfoil were validated using the CFD method outlined in Ullah's [12]. This validation provides confidence that the XFLR5 v 6.61 results are accurate and can be used for further analysis and interpretation.

To summarize, a comparison of several airfoil designs at low Re numbers reveals both consistent trends and large variances in aerodynamic efficiency. The observed trends in Cl and lift-to-drag ratio demonstrate the complicated interplay between AOA, airfoil geometry, and overall aerodynamic performance. These insights contribute to a full understanding of the indirect implications that certain design alterations might have on airfoil performance under various operating conditions.

More research could look into the impact of airfoil geometry changes on performance throughout a broader range of Re numbers, including low and high values, in order to optimize VTOL UAV aerodynamics. Furthermore, a better understanding

of the complex relationships between airfoil design and aerodynamic efficiency in subsonic flight conditions is necessary.

4. Conclusion

This study investigated the effects of airfoil geometry at low Re numbers on the aerodynamic characteristics of flying wing UAVs, with a particular emphasis on 1×10^6, 2×10^6, and 5×10^6. This research provides new insights into critical areas of the aerodynamic performance of VTOL UAVs during subsonic flight situations by thoroughly analyzing various airfoil designs.

The NACA 6409 is a noteworthy airfoil due to its outstanding performance at all tested Re numbers. The airfoil continuously showed greater Cl_{max} and favorable stall angles, which are indicators of superior aerodynamic efficiency. The results concerning drag divergence, in particular the determination of particular angles at which abrupt increases in drag take place, offer fresh perspectives on stalling behavior and underscore the possibility for optimal performance of NACA 6409 in VTOL UAV applications.

The unique contribution of this study is the thorough comparison of airfoil performance, which shows that the NACA 6409 is suitable for low-speed UAV operations because it not only maintains maximum aerodynamic efficiency at different Re numbers but also reaches a peak lift-to-drag ratio at 1×10^6. These findings support the robustness and versatility of the aerodynamic properties of the NACA 6409 airfoil, with important implications for UAV design in the future.

The study's conclusions also emphasize the significance of comprehending the subtle variations in lift-to-drag ratios among different airfoils, leading to a more complex knowledge of how geometric variables affect overall aerodynamic performance. This work establishes the foundation for future developments in airfoil design specifically suited to the particular difficulties of low Re number flight and implies that more investigation over a wider range of Re numbers may contribute to a deeper understanding of VTOL UAV aerodynamics. By doing so, UAV technology would advance and a more thorough grasp of the intricate relationship between aerodynamic efficiency and airfoil design would be fostered.

Ethical Statement

This study does not contain any studies with human or animal subjects performed by any of the authors.

Conflicts of Interest

The authors declare that they have no conflicts of interest to this work.

Data Availability Statement

Data available on request from the corresponding author upon reasonable request.

Author Contribution Statement

Timothy A. Adeyi: Conceptualization, Software, Resources, Writing – original draft. **Oluwaseyi O. Alabi:** Methodology, Validation, Formal analysis, Investigation, Data curation, Writing – review & editing. **Olumide A. Towoju:** Visualization, Supervision, Project administration.

References

[1] Saikhom, V., & Kalita, M. (2023). Advancements in UAV remote sensing: A comprehensive review. *Journal of Survey in Fisheries Sciences*, *1*(1), 1355–1360.

[2] Saravanakumar, Y. N., Sultan, M. T. H., Shahar, F. S., Giernacki, W., Łukaszewicz, A., Nowakowski, M., . . . , & Stępień, S. (2023). Power sources for unmanned aerial vehicles: A state-of-the art. *Applied Sciences*, *13*(21), 11932.

[3] Baube, C. A., Downs, C., Goodstein, M., Labrador, D., Liebergall, E., & Molloy, O. (2024). Fli-Bi UAV: A unique surveying VTOL for overhead intelligence. In *AIAA SCITECH 2024 Forum*, 0455.

[4] Misra, A., Jayachandran, S., Kenche, S., Katoch, A., Suresh, A., Gundabattini, E., . . . , & Legesse, A. A. (2022). A review on vertical take-off and landing (VTOL) tilt-rotor and tilt wing unmanned aerial vehicles (UAVs). *Journal of Engineering*, *2022*, 1803638.

[5] Kiesewetter, L., Shakib, K. H., Singh, P., Rahman, M., Khandelwal, B., Kumar, S., & Shah, K. (2023). A holistic review of the current state of research on aircraft design concepts and consideration for advanced air mobility applications. *Progress in Aerospace Sciences*, *142*, 100949.

[6] Healy, F., Cheung, R., Rezgui, D., Cooper, J., Wilson, T., & Castrichini, A. (2023). On the effect of geometric nonlinearity on the dynamics of flared folding wingtips. *Journal of Aircraft*, *60*(2), 368–381.

[7] Darvishpoor, S., Roshanian, J., Raissi, A., & Hassanalian, M. (2020). Configurations, flight mechanisms, and applications of unmanned aerial systems: A review. *Progress in Aerospace Sciences*, *121*, 100694.

[8] Coelho, V. (2021). *Aerodynamic detailed design of an unmanned aerial vehicle with VTOL capabilities*. Doctoral Dissertation, Academia da Força Aérea.

[9] Raja, V., Murugesan, R., Solaiappan, S. K., Arputharaj, B. S., Rajendran, P., AL-bonsrulah, H. A., . . . , & Ketema, A. (2023). Design, computational aerodynamic, aerostructural, and control stability investigations of VTOL-configured hybrid blended wing body-based unmanned aerial vehicle for intruder inspections. *International Journal of Aerospace Engineering*, 2023, 9699908.

[10] Coder, J. G., & Maughmer, M. D. (2014). Comparisons of theoretical methods for predicting airfoil aerodynamic characteristics. *Journal of Aircraft*, *51*(1), 183–191.

[11] Jones, G., Santer, M., Debiasi, M., & Papadakis, G. (2018). Control of flow separation around an airfoil at low Reynolds numbers using periodic surface morphing. *Journal of Fluids and Structures*, *76*, 536–557.

[12] Ullah, S. (2019). Analysing India's naval development strategy. *IPRI Journal*, *19*(1), 103.

[13] Marques, M. N., Magalhães, S. A., Dos Santos, F. N., & Mendonça, H. S. (2023). Tethered unmanned aerial vehicles—A systematic review. *Robotics*, *12*(4), 117.

[14] Bowman, E. K., & Zimmerman, R. J. (2015). *US Army Research Laboratory joint interagency field experimentation 15-2 final report*. Adelphi: ARL.

[15] Chaturvedi, S. K., Sekhar, R., Banerjee, S., & Kamal, H. (2019). Comparative review study of military and civilian unmanned aerial vehicles (UAVs). *INCAS Bulletin*, *11*(3), 181–182.

[16] Yadav, A. R., Mehta, D., Belani, J., Chauhan, R. R., & Ajay Vishwath, N. C. (2022). A guide to novice for proper

selection of the components of drone for specific applications. *Materials Today: Proceedings*, *65*, 3617–3622.

[17] Lushenko, P. (2022). US Presidents' use of drone warfare. *Defense & Security Analysis*, *38*(1), 31–52.

[18] Nichols, R. K., Mumm, H., Lonstein, W. D., Ryan, J. J., Carter, C. M., Hood, J. P., . . . , & Jackson, M. J. (2020). *Unmanned vehicle systems & operations on air, sea, land*. USA: New Prairie Press.

[19] Nichols, R. K., Mumm, H. C., Lonstein, W., Sincavage, S., Carter, C. M., Hood, J. P., . . . , & Shields, B. (2021). *Disruptive technologies with applications in airline & marine and defense industries*. USA: New Prairie Press.

[20] Jha, S. K., Prakash, S., Rathore, R. S., Mahmud, M., Kaiwartya, O., & Lloret, J. (2022). Quality-of-service-centric design and analysis of unmanned aerial vehicles. *Sensors*, *22*(15), 5477.

[21] Maji, A., Pandi, J. S. S., & Mittal, S. (2024). Aerodynamic center of a wing at low Reynolds number. *Physics of Fluids*, *36*(3), 1–17.

[22] Sagaut, P., & Deck, S. (2009). Large eddy simulation for aerodynamics: Status and perspectives. *Philosophical Transactions of the Royal Society A: Mathematical, Physical and Engineering Sciences*, *367*(1899), 2849–2860.

[23] Kakade, S., Chikkala, D., Reghunath, K., & Seeni, A. (2022). Aerodynamic analysis and optimization of wings for the Jain University sailplane using XFLR5. *ECS Transactions*, *107*(1), 493.

[24] Rosescu, J. (2020). *A study of the design of adaptive camber winglets*. Doctoral Dissertation, California Polytechnic State University.

[25] Haque, A. U., Asrar, W., Omar, A. A., Sulaeman, E., & Ali, M. J. (2016). A novel technique to neutralize the Yawing moment due to asymmetric thrust in a hybrid buoyant aircraft. In *EPJ Web of Conferences* (Vol. 114, p. 02128). EDP Sciences.

[26] Mehdi, H., Gaurav, S., & Sharma, M. (2016). Numerical investigation of fluid flow and aerodynamic performance on a 2D NACA-4412 airfoil. *International Journal of Research in Engineering and Innovation*, *1*(1), 5.

How to Cite: Adeyi, T. A., Alabi, O. O., & Towoju, O. A. (2024). Influence of Airfoil Geometry on VTOL UAV Aerodynamics at Low Reynolds Numbers. *Archives of Advanced Engineering Science*. https://doi.org/10.47852/bonviewAAES42023485